Environmental Fluid Mechanics (2022) 22:275–300
https://doi.org/10.1007/s10652-021-09797-3

ORIGINAL ARTICLE

Free surface profiles of near-critical instabilities in open channel flows: undular hydraulic jumps

Oscar Castro-Orgaz[1] · Hubert Chanson[2]

Received: 11 May 2021 / Accepted: 8 June 2021 / Published online: 19 June 2021

Abstract

When the Froude number F of a free-surface flow ranges between 0.3 and 3, the flow is unstable and frequently characterised by free surface undulations, with the undular hydraulic jump being a seminal flow in hydro-environmental mechanics. The presence of the free surface undulations significantly affects the flow field, with major velocity and pressure field redistributions between successive crests and troughs. All the current theoretical models to simulate undular hydraulic jumps are limited to two-dimensional flow conditions, ignoring all the relevant three-dimensional flow effects, namely shock-wave drag, turbulent breaking and turbulent stresses. These aspects are critically accounted for in this review article, where a depth-averaged Boussinesq model which approximately accounted for 3D flow effects was presented, constituting the first attempt in this line. The model predictions were compared with experimental results from different sources for $F_1 < 1.5$, with F_1 the inflow Froude unnumber, resulting a reasonable agreement with observations. The curvature distribution parameter was found to controlling the wave length, and an approximate value was obtained based on ideal fluid flow computations. The new depth-averaged model did not include the effect of flow concentration in the centerline, observed physically, but this 3D feature is analysed at the first wave crest based on an improved treatment of flow curvature, highlighting the impact of the ratio q_{CL}/q on the velocity profile features with q_{CL} the centerline discharge. The main limitation of the new model, presented in this critical review, originated from approximating a complex 3D flow by a depth-averaged model. However, the predictions with the new approximate treatment of 3D effects produced better results than those previously reported.

Keywords Boussinesq-type models · Free surface instabilities · Hydraulic jumps · Near-critical flows · Undular flows

✉ Oscar Castro-Orgaz
ag2caoro@uco.es

Hubert Chanson
h.chanson@uq.edu.au

[1] University of Cordoba, Spain, Campus Rabanales, Leonardo Da Vinci Building, 14071 Cordoba, Spain

[2] The University of Queensland, School of Civil Engineering, Brisbane, QLD 4072, Australia

1 Introduction

When the Froude number F of a free-surface flow ranges between 0.3 and 3, the relationship between specific energy and flow depth reveals that a small change in energy can produce a large change in the flow depth [1–5]. The flow is thus unstable and often characterised by the development of free-surface undulations. These flows are called "near-critical flows", and examples of unstable undular flows in hydro-environmental problems are the undular hydraulic jump and the undular surge [6].

The free surface undulations might produce overtopping and damage in the channel banks. The propagation of large waves over very long distances might also disrupt navigation, pump or turbine operation, induce unnecessary vibrations to downstream structures, e.g. locks and gates, or disturb discharge measurements at downstream discharge meter structures [7–10]. The presence of undular flow modifies considerably the flow field and hence the turbulent mixing in a channel [11, 12]. Existing numerical models of turbulent mixing and transport should not be used for undular jump flows. Computational models based on the Saint Venant equations are not adequate to predict undular flows. For undular jumps even models based on the Serre–Green–Nagdhi (SGN) equations [13–15] are not adequate, given that they are based on ideal fluid flow velocity and pressure distributions [16, 17]. For undular surges, however, this is a reasonably good approximation. Although SGN models are modified to accommodate boundary friction effects in the streamwise momentum balance, the redistributions of velocity and pressure at wave extrema remains essentially identical to that of ideal fluid flows [13, 18]. Thus, undular jumps can only be modeled with a turbulent flow approach, whereas for the undular surge ideal fluid flow computations are acceptable [19–21]. This dispels the notion that the undular jump is a steady undular surge: both are different flows, one is highly turbulent, the other close to ideal [1]. Castro-Orgaz and Chanson [22] presented detailed computations of undular surges using SGN theory, such that focus of this review is on the stationary undular hydraulic jump.

In an undular hydraulic jump, the vertical pressure distribution is not hydrostatic beneath the free-surface undulations. The pressure gradient is larger than hydrostatic at each wave trough and smaller at each wave crest [23, 24]. This observation is consistent with the curvature of the free-surface and ideal fluid flow considerations [25–27]. Significant velocity redistributions are observed between crest and trough [11, 28]. However, ideal fluid flow computations are unable to predict the velocity profile of the undular jump [29]: A significant reduction of velocity towards the channel bottom

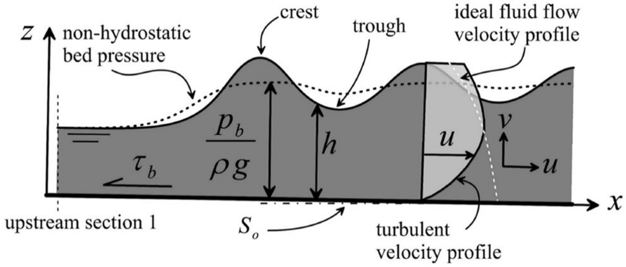

Fig. 1 Definition sketch of free surface profile of 2D undular hydraulic jump, or centerline profile for a 3D jump, with flow direction from left to right. Non-hydrostatic fluid bottom pressure and turbulent velocity profile features are highlighted

is observed at a wave crest, just the opposite trend predicted by ideal fluid flow computations (Fig. 1). It indicates that boundary shear greatly affects the velocity profile of undular hydraulic jumps. Thus, both non-hydrostatic pressure and boundary shear effects shall be accounted for in undular jump simulation models [30]. Note that undular flows may be greatly affected by small changes in boundary friction, e.g., for identical upstream Froude number and aspect ratio, a modification of sidewall roughness modifies substantially the shape and properties of the undular hydraulic jumps [28]. The flow characteristics are significantly affected by the inflow conditions (fully-developed or partially-developed) and by the aspect ratio defined as the ratio of the channel width to the critical depth [30–32].

The undular hydraulic jump involves a two-dimensional (2D) velocity field with a 1D free surface for $F_1 < 1.2$ (roughly) with F_1 as the inflow Froude number, [11] (Fig. 1). Along the channel sidewalls. boundary layers are developed under an adverse pressure gradient [1] (Fig. 2). For increasing values of F_1, lateral shockwaves develop due to flow separation along the sidewalls, resulting in a 3D velocity field and a 2D flow surface (Fig. 2) [11, 31, 33–35]. The first significant theoretical and experimental research work on the undular hydraulic jump was conducted by Fawer [29].

Experimental observations indicated five different types of undular hydraulic jumps [11, 23], with the limiting value of F_1 between each class dependent on the aspect ratio h_c/b, where h_c is the critical depth and b the channel width. For channels with low aspect ratio the first intersection of shock waves occurs at the first wave crest [23], whereas for a wide aspect ratio this occurs beyond [35]. For low aspect ratio ($h_c/b < 0.1$), the classification of undular jumps is as follows [11]:

Type A: Two-dimensional flow structure without shock waves; $F_1 < F_A = 1.22$.
Type B: Shock waves develop but wave breaking is absent at their intersection; $F_1 < F_B = 1.72$
Type C: Wave breaking is detected at the intersection of shockwaves, but air entrainment is absent; $F_1 < F_C = 2.1$
Type D: Air entrainment is evident at the shock wave intersection; $F_1 < F_D = 2.4$

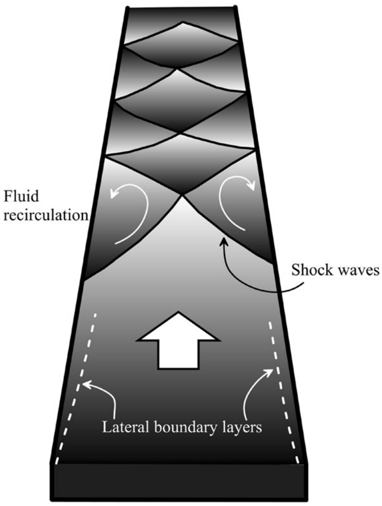

Fig. 2 Spatial view of non-breaking undular jump looking downstream, showing the shock-waves and fluid recirculation. Shock waves start at the point of separation of the lateral boundary layers forming on the channel sidewalls, which are subjected to an adverse pressure gradient

Type E: The roller developed at the first shock-wave intersection widens and the undulations disappear from the flow profile; $F_1 > F_D = 2.6$

In general, the limiting F-values for each jump type decrease with increasing h_c/b values. For example, with $F_1 = 1.3$ and $h_c/b = 0.4$ it is possible to obtain a C or D jump type [23]. Further, the limiting value for breaking jumps F_C is in addition sensitive to the bottom slope, as discussed by Gotoh et al. [35]. The subject matter is extremely complex and so far there is not yet a universal classification, given the many factors affecting the undular jump profile.

Furthermore, the inherent 3D nature of the flow field within the undular hydraulic jump is best noted considering the unit discharge at the centerline q_{CL}, obtained by integration of the experimental velocity profiles, as compared to the average discharge per unit channel width q supplied at the flume inlet. The ratio q_{CL}/q was experimentally determined by Chanson [23] along undular hydraulic jumps, resulting values significantly above unity, implying some flow concentration about the channel centerline. The longitudinal variations of the ratio q_{CL}/q further showed a marked undulating pattern in the streamwise direction, mimicking the wave crests and troughs of the jump profile. This increased centerline unit discharge originates from the lateral mass transfer, which tend to concentrate the flow on the flume axis. At the wave crests the effect is larger, with ratios easily of the order of 1.5. At the wave troughs the ratio is also above unity, but not as high as at the wave crests.

The modelling approach for undular hydraulic jumps is based on the work of Boussinesq [36], given the significant impact of non-hydrostatic fluid pressure. Fawer [29] applied the ideal fluid flow theory and obtained an extended Boussinesq-type energy equation with an undetermined flow curvature parameter. Once approximated, the development was used to analyse the tailwater cnoidal-type waves of the undular jump. Iwasa [37], Mandrup-Andersen [38] and Hager and Hutter [39] approximated the undular hydraulic jump profile with a composite potential curve matching a solitary wave with a cnoidal wave at an arbitrary point based on the work by Benjamin and Lighthill [40]. At the joining point a slope discontinuity on the free surface profile is formed, given the impossibility of the potential flow theory of transforming the upstream supercritical flow into a subcritical tailwater flow. Marchi [18] included frictional effects in the streamwise energy balance via use of the friction slope and the corresponding flow resistance equations. This mathematical model was proposed by Serre [13]. Some improvements are obtained allowing for the variation of the energy head with friction, but other fundamental flow features, like the turbulent velocity profile, remains unexplained by this basic pseudo-potential theory. This model was extensively tested by Castro-Orgaz and Chanson [41] for undular hydraulic jumps and undular weir flows. Fawer [29] measured the velocity profiles along undular jumps, with the experimental results significantly differing from those originating from the potential flow theory (Fig. 1). This important experimental finding suggests the need of including boundary shear effects into the development of Boussinesq-type velocity and pressure distributions for undular flows, as noted by Montes [1], Montes and Chanson [30], and Bose et al. [42]. Hosoda and Tada [43] and Hosoda et al. [44] used a Boussinesq-type momentum equation with non-hydrostatic terms resulting from the potential flow theory. They introduced boundary shear effects only into the streamwise momentum balance and considered in addition the effect of turbulence. They implemented in the streamwise depth-averaged momentum equation the turbulent normal stresses using a depth-averaged eddy viscosity. The development is therefore a modification of Serre [13] theory allowing for the effect of turbulence. Grillhofer and Schneider [45] applied a perturbation method to study undular jump profiles, and Castro-Orgaz [46] analysed different skin friction formulae for Boussinesq equations. Castro-Orgaz et al. [47] simulated the turbulence in a Boussinesq equation by a standard depth-averaged k-ε model.

All the existing models to simulate undular hydraulic jumps are limited to $F_1 < 1.2$, given the 2D developments ignoring the sidewall friction effect, and, so far, there has not been any attempt in the literature to introduce, approximately, all the relevant 3D flow effects, namely shock-wave drag, turbulent breaking and turbulent stresses, into the 2D Boussinesq-type approach with boundary shear effects.

Free-surface undulations, e.g. as in undular jumps, are indications that the flow conditions are unstable, that is, near-critical or transcritical. The presence of the free surface undulations significantly affects the flow field, with important velocity and pressure field redistributions between successive crest and trough. None of the modeling approaches available attempted to introduce 3D effects approximately, limiting the models to $F_1 < 1.2$. These aspects are critically accounted for in this review article. Focus is on the undular jump profile and the approximate inclusion of the effects of shock-waves and turbulence in the 2D Boussinesq equations with some boundary shear.

2 Extended 2D open channel flow equations and numerical method of solution

2.1 Theory

The development of extended channel flow equations for undular flows starts by considering the ideal fluid flow velocity distribution for a straight-bottomed channel as [30]

$$V = V_s \exp\left(-\frac{hh_{xx}}{1+h_x^2}\frac{1-\mu^{K+1}}{K+1}\right) = V_s \exp\left(-\varepsilon_0 \frac{1-\mu^{K+1}}{K+1}\right), \tag{1}$$

where V_s is the velocity at the free surface, $\mu = z/h$, z the elevation, h the flow depth, K the curvature parameter, $h_x = \mathrm{d}h/\mathrm{d}x$ and $h_{xx} = \mathrm{d}^2h/\mathrm{d}x^2$. The curvature term is $\varepsilon_0 = hh_{xx}/(1+h_x^2)$. The exponent K determines the depth-variation of streamline curvature, with typical values ranging from 0.5 to 2 [29]. This velocity profile is basically the result of Fawer [29], which, however, was found to diverge from observations in undular jumps due to shear effects. The starting 2D model in this review considers the development of Montes and Chanson [30], namely,

$$V = V_s \mu^N \exp\left(-\varepsilon_0 \frac{1-\mu^{K+1}}{K+1}\right), \tag{2}$$

thereby introducing boundary shear effects in undular flows by a Prandtl-type power law damping with exponent N. Castro-Orgaz and Hager [48] demonstrated that Eq. (2) is an analytical solution of Bernoulli equation along a streamline with the inflow vorticity prescribed using N. Equation (2) produces the following kinematic field (u, v) by projecting in the (x, z) directions [30]

$$u = (1+N)\frac{q}{h}\mu^N\left[1 - \frac{\varepsilon_0}{K+1}\left(\frac{1+N}{K+2+N} - \mu^{K+1}\right) - \frac{\varepsilon_1}{2}\left(\frac{N+1}{N+3} + \mu^2\right)\right], \tag{3}$$

$$v = (1+N)\frac{q}{h}\mu^{N+1}\varepsilon_1^{1/2}\left[1 - \frac{\varepsilon_0}{K+1}\left(\frac{1+N}{K+2+N} - \mu^{K+1}\right) - \frac{\varepsilon_1}{2}\frac{N+1}{N+3}\right], \tag{4}$$

where the slope term $\varepsilon_1 = {h_x}^2/(1+{h_x}^2)$ and q is the unit discharge. The vertical pressure distribution derived from this velocity field is [30]

$$\frac{p}{\rho g h} = 1 - \mu + \frac{\varepsilon_0 (1+N)^2}{K+2N+1}\frac{q^2}{gh^3}\left(1 - \mu^{1+2N+K}\right). \tag{5}$$

Equations (3)–(5) can be used to obtain the specific momentum S and depth-averaged specific energy E of undular flows, resulting (Appendix)

$$S = \frac{h^2}{2} + \beta\frac{q^2}{gh}\left[1 + \varepsilon_0\left(\frac{2}{K+N+2} - \frac{1-2N}{K+2N+2} +\right) - \varepsilon_1\left(\frac{N+1}{N+3}\right)\right], \tag{6}$$

$$E = h + \beta\frac{q^2}{2gh^2}\left[1 + \frac{2\varepsilon_0}{K+2N+2}\left\{1 + N\left(2 + \frac{1}{K+N+2}\right)\right\} - \varepsilon_1\left(\frac{N+1}{N+3}\right)\right], \tag{7}$$

with $\beta = (1+N)^2/(1+2N)$ as the Boussinesq velocity correction coefficient. The variations of these quantities along the undular jump profile are determined by the depth-averaged balances:

$$\frac{\mathrm{d}S}{\mathrm{d}x} = h\left(S_o - S_f\right), \tag{8}$$

$$\frac{\mathrm{d}E}{\mathrm{d}x} = S_o - S_f, \tag{9}$$

where S_o is the bottom slope and S_f the friction slope. The friction slope is derived from the Darcy-Weisbach equation for a rectangular section of width b as

$$S_f = \frac{\tau_b}{\rho g R_h} = \frac{f}{4R_h}\frac{U^2}{2g} = \frac{f}{8}\left(1 + 2\frac{h}{b}\right)\mathrm{F}^2. \tag{10}$$

Here τ_b is the bed shear stress, $U = q/h$ the depth-averaged velocity, R_h the hydraulic radius, f the Darcy-Weisbach friction factor and F the local Froude number. For a given value of K, closure for the bed shear effects, namely N and f, is needed for numerically solving either Eqs. (6) and (8) or (7) and (9) for momentum and energy, respectively. Montes and Chanson [30] proposed the boundary layer method of Furuya and Nakamura [49] for adverse pressure gradients, like those occurring in undular hydraulic jumps. The model equations considered in the ensuing development are valid for fully-developed flows. The first boundary-layer equation is von Kármán equation [30, 50]

$$\frac{\mathrm{d}\theta}{\mathrm{d}x} = -\frac{\theta}{U_e}\frac{\mathrm{d}U_e}{\mathrm{d}x}(H+2) + \frac{C_f}{2}. \tag{11}$$

Here θ is the boundary layer momentum thickness, U_e is the maximum velocity at the boundary layer edge $\approx (1+N)(q/h)$, H is the shape factor $= 1 + 2N$, and $C_f = \tau_b/(\rho {U_e}^2/2)$ the skin-friction coefficient. Note that by definition C_f and f are thus related by

$$f = 4C_f(1+N)^2. \tag{12}$$

The second boundary-layer equation is a transport equation for $k=u_\theta/U_e$, the ratio of velocity at the momentum thickness to boundary layer edge, given by [30, 49]

$$\frac{\mathrm{d}k}{\mathrm{d}x} = 1.46\frac{1-k^2}{(1.5+k)\theta\,\mathrm{R}_\theta^{1/4}}[\Gamma + 0.118(0.67-k)], \tag{13}$$

with $\Gamma=(\theta/U_e)(\mathrm{d}U_e/\mathrm{d}x)\mathrm{R}_\theta{}^{1/4}$ as Buri's shape factor, $\mathrm{R}_\theta=(U_e\theta)/\nu=[\mathrm{R}_1(1+N)\theta)]/h$ the momentum thickness Reynolds number and $\mathrm{R}_1=q/\nu$ as the approach-flow Reynolds number, where ν is the kinematic viscosity of water. The skin-friction coefficient C_f is determined by the Ludwieg and Tillman correlation as [50]

$$C_f = 0.246\mathrm{R}_\theta^{-0.268}\times 10^{-0.678H}. \tag{14}$$

The shape factor H is determined from k by using the correlation [30, 49]

$$H = \left[1.3 + 1.3(0.7-k) + 3(0.7-k)^2\right]^{2/3}. \tag{15}$$

Once H is known, the velocity exponent follows from $N=(H-1)/2$. The acceleration term is estimated as

$$\frac{\mathrm{d}U_e}{\mathrm{d}x} = U\frac{\mathrm{d}N}{\mathrm{d}x} - (1+N)\frac{U}{h}\frac{\mathrm{d}h}{\mathrm{d}x}, \tag{16}$$

which permits to rewrite Eq. (11) as

$$\frac{\mathrm{d}\theta}{\mathrm{d}x} = -\theta\left(\frac{1}{2+2N}\frac{\mathrm{d}H}{\mathrm{d}x} - \frac{1}{h}\frac{\mathrm{d}h}{\mathrm{d}x}\right)(H+2) + \frac{C_f}{2}. \tag{17}$$

Here the derivative $\mathrm{d}H/\mathrm{d}x$ was determined from Eq. (15) analytically.

2.2 Numerical implementation

In this work we will consider momentum-based solutions, given that the forthcoming inclusion of 3D flow features is more straightforward. For 2D jumps ($\mathrm{F}_1<1.2$) both the energy and momentum systems were found to give similar results. Equations (6), (8), (17) and (13) form the following momentum-based system of ODEs for the unknowns $h(x)$, $h_x(x)$, $S(x)$, $\theta(x)$ and $k(x)$:

$$\frac{\mathrm{d}\mathbf{f}}{\mathrm{d}x} = \mathbf{g}, \tag{18}$$

where:

$$\mathbf{f}=\begin{pmatrix}h\\h_x\\S\\\theta\\k\end{pmatrix},\quad \mathbf{g}=\begin{pmatrix}h_x\\ \left[\frac{gh}{\beta q^2}\left(S-\frac{h^2}{2}\right)-1+\varepsilon_1\left(\frac{N+1}{N+3}\right)\right]\Big/\left[\frac{h}{1+h_x^2}\left(\frac{2}{K+N+2}-\frac{1-2N}{K+2N+2}\right)\right]\\ h\left(S_o-S_f\right)\\ -\theta\left(\frac{1}{2+2N}\frac{\mathrm{d}H}{\mathrm{d}x}-\frac{1}{h}\frac{\mathrm{d}h}{\mathrm{d}x}\right)(H+2)+\frac{C_f}{2}\\ 1.46\frac{1-k^2}{(1.5+k)\theta\,\mathrm{R}_\theta^{1/4}}[\Gamma+0.118(0.67-k)]\end{pmatrix}.$$

Starting with the values of $\mathbf{f}=(h, h_x, S, \theta, k)^{\mathrm{T}}$ at a section x these variables are computed at a new position $x+\Delta x$ with the 4th-order Runge–Kutta method [5, 51], with Δx as the space step. Montes [1] reported computational difficulties solving extended systems of this kind by employing different ODE solvers. Our Runge–Kutta solver was found to be robust and accurate, so other methods as Hamming's third-order one [30] were not considered further. The streamwise evolutions of $H(x)$, $N(x)$, $Cf(x)$, $f(x)$ are produced as part of the solution: H is determined from k by resorting to Eq. (15); N is determined as $(H-1)/2$; C_f is determined from Eq. (14) once R_θ is evaluated, and f is determined from Eq. (12). The boundary conditions at the toe of the undular jump (Sect. 1, see Fig. 1) are as follows. For a given value of F_1 the flow depth is $h_1=h_c\mathrm{F}_1^{-2/3}$. The curvature term h_{xx} is set to zero, and h_x varied from 0.001 to 0.01 by choice to deviate the flow from uniform flow conditions. Based on the experimental velocity profile at Sect. 1 the exponent N_1 is determined. The value S_1 is then deduced from Eq. (6). The momentum thickness is for fully-developed shear flow at 1 $\theta_1=(N_1h_1)/[(2N_1+1)(N_1+1)]$, and the shape factor $H_1=2N_1+1$. The value k_1 is deduced from Eq. (15) using H_1. To run the solver a suitable value of the curvature parameter K is necessary. This issue is dealt with in the next section.

3 Estimation of curvature parameter

Fawer [29] considered that the curvature of streamlines obeys a non-linear variation with depth by introducing a curvature parameter K. A typical approach in curvilinear open channel flows is $K=1$, that is, assuming a linear variation of streamline curvature [30]. However, this is not necessarily the best approach. Indeed, several experimental studies showed

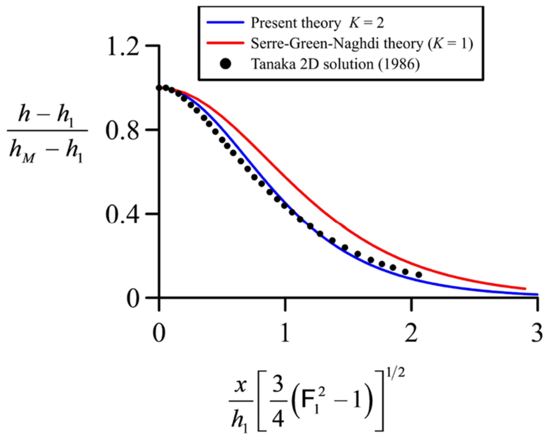

Fig. 3 Determination of curvature parameter K of present theory for solitary wave of maximum height $(h_M-h_1)/h_1=0.65$

that the characteristics of the first wave differed from the ensuing waves [11, 52]. The first wave of an undular hydraulic jump presents some analogies with the solitary wave profile [18, 37], and, thus, it will be used here as idealized test case to select a suitable value of K. For $K=1$, $\varepsilon_0 \approx hh_{xx}$ and $\varepsilon_1 = {h_x}^2$ the present theory yields, with the boundary condition $h_x \to 0$ for $h \to h_1$ [13, 40, 53]

$$\frac{h}{h_1} = 1 + \left(\mathrm{F}_1^2 - 1\right)\mathrm{sech}^2\left[\frac{\left(3\mathrm{F}_1^2 - 3\right)^{1/2}}{\mathrm{F}_1}\frac{x}{2h_1}\right], \tag{19}$$

which is the solitary wave solution of the Serre–Green–Naghdi (SGN) equations.

Equation (19) is plotted in Fig. 3 for a solitary wave of maximum normalized height $(h_M - h_1)/h_1 = 0.65$, which is a highly non-linear wave close to the maximum possible. Here h_M is the maximum (crest) flow depth, given by SGN theory as $h_M = h_1 {\mathrm{F}_1}^2$. The exact 2D potential flow solution obtained by Carter and Cienfuegos [54] using the method of Tanaka [55], based on the simultaneous solution of Bernoulli's equation along the free surface and a boundary integral equation obtained from Cauchy's theorem, is also included. As discussed by Carter and Cienfuegos [54], the solitary wave solution of the SGN equations yields waves which are too wide as compared to 2D results. Therefore, $K=1$ is not the best choice in the context of the present research.

The numerically generated solitary wave profile from the present theory for $K=2$ is plotted in Fig. 3, showing a narrower wave profile and thus better agreement with the Tanaka [55] 2D solution. Thus, this value is selected for simulation of the undular jump profile. To further test the adequacy of the selected value for K, the full 2D solution of the irrotational velocity field (u, v) was determined using the x-ψ method [56–58] for comparison purposes with the approximate 2D velocity field given by Eqs. (3) and (4) for $N=0$ and $K=2$. The free surface streamline was prescribed using the solitary wave profile previously obtained from the present theory, and the flow field was numerically determined by solving the Laplace equation of the x-ψ method using a finite difference scheme:

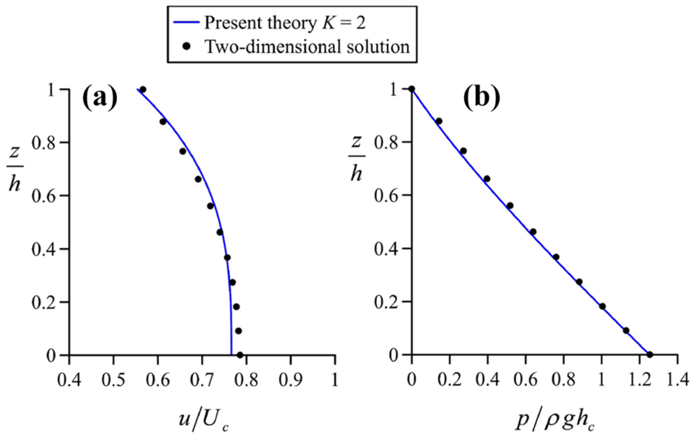

Fig. 4 Distributions of horizontal velocity u/U_c and pressure $p/(\rho g h_c)$ at crest of solitary wave of maximum height $(h_M - h_1)/h_1 = 0.65$, with U_c and h_c as the critical velocity and depth, respectively

$$\nabla^2 z = \frac{\partial^2 z}{\partial x^2}\left(\frac{\partial z}{\partial \psi}\right)^2 + \frac{\partial^2 z}{\partial \psi^2}\left[1+\left(\frac{\partial z}{\partial x}\right)^2\right] - 2\frac{\partial^2 z}{\partial x \partial \psi}\frac{\partial z}{\partial x}\frac{\partial z}{\partial \psi} = 0, \tag{20}$$

where ψ is the stream function. Details of the numerical method are extensively described by Montes [57, 58]. The up- and downstream boundary sections were located at $x/h_c = \pm 5$, and the flow was modelled using 11 streamlines. Once Eq. (20) is solved, the velocity field (u, v) was obtained by differentiation of the numerical values of the stream function. The pressure distribution was determined from the computed velocity field using Bernoulli equation.

The computed 2D vertical distributions for u/U_c and $p/(\rho g h_c)$ at the solitary wave crest are plotted in Fig. 4 and compared with the results obtained from Eqs. (3) and (4) for $N=0$ and $K=2$. Note some deviations between both methods. However, given many other factors extremely difficult to quantify in undular hydraulic jumps, the approximate results obtained from $K=2$ are considered adequate.

4 Approximate treatment of 3D effects

4.1 Shock waves

Shock waves (Fig. 5) are formed in undular hydraulic jumps just downstream from the inflow section once the lateral boundary layers, growing under an adverse pressure gradient, separate, and recirculation flow zones are formed (Fig. 2). The shock waves constitute some kind of flow separation at the sidewalls, with recirculation observed immediately downstream of shock wave near the free-surface [23, 59]. These cross waves intersect at the first wave crest for low aspect ratios, being further reflected at the walls and intersecting several times downstream along the flume. For $F_1 < 1.2$ the rise in the water surface profile up to the first wave crest does not produce the necessary pressure gradient to produce separation and then the conditions for shock wave development. Montes and Chanson [30] analysed the energy loss in the undular jump profile up to the first wave crest, dividing it into a component due to the shock waves and another due to turbulence and boundary shear. Both were found to be equally important, and, although the relative energy loss in the undular jump is not as high as in a normal hydraulic jump, it is strong enough to significantly affect the undular jump profile. In fact, there is a narrow region in the energy–momentum diagram of Benjamin and Lighthill [40] where the undular jump profile exits [1], thus the

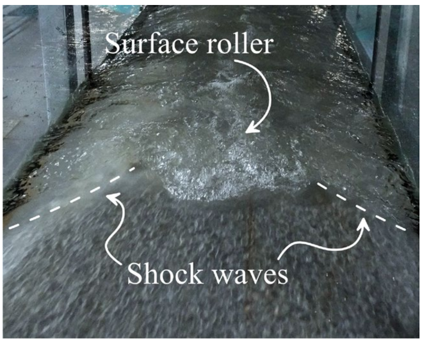

Fig. 5 Undular jump with shock waves and roller at first wave crest (Type D–E) in the 19 m long rectangular channel at UQ, looking downstream with flow direction from foreground to background; $Q=0.0265$ m^3/s, $S_o=1.25\%$, $b=0.7$ m, $h_1=3.2$ cm, $F_1=2.1$

importance of carefully quantifying the energy loss. Basically, the shock waves produce an increase in drag, with a force D estimated by analogy to aerodynamic flows as [30]

$$D = \frac{1}{2}\rho c_D U^2 (\mathrm{F} - 1)^4, \tag{21}$$

where c_D is a drag coefficient. Manipulation of this result permits to write a drag slope S_D as [30]

$$S_D = \frac{1}{2} c_D \mathrm{F}^2 (\mathrm{F} - 1)^4. \tag{22}$$

Inclusion of Eq. (21) in undular jump profile computations will be done by adding S_D to the streamwise momentum balance [Eq. (8)]. Thus, the drag-enhancing effect of the shock waves will be accounted for. The implementation will be drastically simplified as follows. Given that the exact position of shock wave start is not known in advance, it will be assumed that it is coincident with the inflow section. This approximation is close to experimental observations [52]. Further, it will be assumed that the first intersection of shock waves occurs at the first wave crest, which will be the case for low aspect ratios. Therefore, S_D will be accounted for from the initial section up to the first wave crest, and set to $S_D = 0$ downstream of it. Based on the test data by Montes and Chanson [30] a value $c_D = 0.01$ was adopted for the computations, although it is also dependent on F_1. However, given that the approximate treatment of 3D effects, further refinements were not attempted.

4.2 Turbulence

Hydraulic experimentation shows that flow in hydraulic jumps is turbulent, such that any attempt to introduce 3D effects into depth-averaged computations requires its consideration. Turbulence produces basically two important effects to be accounted for in depth-averaged modeling of hydraulic jumps. First, formation of free surface rollers (Fig. 5) produces a deformation of the velocity profile with backward (negative) velocities at the free surface. This distortion of the velocity profile introduces an additional momentum flux, usually neglected in depth-averaged jump models. Second, turbulence provokes the appearance of the Reynolds stresses into the Reynolds-Averaged Navier–Stokes equations, which shall be modelled by a suitable turbulence closure. None of these two effects are accounted for in the SGN equations [13] or in the Montes and Chanson [30] theory. Khan and Steffler [60] considered both effects in direct hydraulic jumps by resorting to an approximate moment model, and obtained good results simulating direct hydraulic jumps ($\mathrm{F}_1 > 2.3$) with a hydrostatic Saint–Venant type model. For undular hydraulic jumps, Castro-Orgaz et al. [47] considered only turbulence by a standard depth-averaged $k{-}\varepsilon$ model, which is not suitable for broken waves. Hosoda et al. [43] considered both wave breaking and Reynolds stresses in undular jumps by approximate procedures, which are, however, very convenient for generalisation of Montes and Chanson [30] theory. These are developed below.

Recent results using the SGN equations [22] and the Vertically-Averaged and Moment (VAM) equations [61] for simulation of undular and broken surges have demonstrated that the momentum flux introduced by velocity profile modeling of breaking waves basically suppresses part of the dispersive effects originating from the non-hydrostatic fluid pressure distribution. This allows for the transition from undular to broken surges. That is, if the velocity profile is modeled for breaking waves in a depth-averaged framework, the effect of the vertical acceleration is attenuated. Modeling the velocity profile is not a simple task, but its bulk effect can be mimicked by an approximate procedure devised by Hosoda and Tada [43]. The basic idea is to establish a threshold of breaking, and once exceed, attenuate the vertical acceleration using a damping factor Ω into the dispersive terms. Hosoda and Tada [43] proposed a damping-factor model based the solitary wave profile. If the ascending branch of the solitary wave profile describes the first wave crest of the undular jump [11, 37], it is possible to find the maximum free surface slope h_x, which occurs at the inflection point. Hosoda and Tada [43] adopted as limiting F_1 for wave breaking 1.25, and, thus, the maximum water surface slope was found to be

$$\left|\frac{\mathrm{d}h}{\mathrm{d}x}\right|_{br} = 0.225. \tag{23}$$

This value is considered a threshold value above which wave breaking occurs. Hosoda and Tada [43] proposed a damping factor Ω given by

$$\Omega = \begin{cases} \exp\left[-\varsigma\left(\left|\frac{\mathrm{d}h}{\mathrm{d}x}\right| - \left|\frac{\mathrm{d}h}{\mathrm{d}x}\right|_{br}\right)\right] & \text{if} \quad \left|\frac{\mathrm{d}h}{\mathrm{d}x}\right| > \left|\frac{\mathrm{d}h}{\mathrm{d}x}\right|_{br} \\ 1 & \text{else} \end{cases} \tag{24}$$

Comparison with laboratory data indicates a calibration parameter $\varsigma = 2$ [43]. Therefore, the non-hydrostatic terms of Montes and Chanson [30] theory ε_0 and ε_1 will be multiplied by Ω. Thus, at any position x of the undular jump the local value of h_x is used to evaluate Eq. (24), such that at breaking nodes $\Omega < 1$. Our computation is therefore adaptative and rather different from the original method from Hosoda and Tada [43], where for a given flow profile the maximum value of h_x was determined and used to compute a single damping factor for all the computational nodes. With the approach pursued here, only those sections with breaking conditions are affected by the exponential damping of dispersive terms.

Turbulent normal stresses are expressed by the time-averaged velocity field (u, v) with k_t as the turbulent kinetic energy and ν_t the eddy viscosity as [60, 62]:

$$\sigma_z = 2\rho\nu_t\frac{\partial v}{\partial z} - \frac{2}{3}\rho k_t, \tag{25}$$

$$\sigma_x = 2\rho\nu_t\frac{\partial u}{\partial x} - \frac{2}{3}\rho k_t. \tag{26}$$

The stress σ_x shall be accounted for in the x-momentum balance whereas σ_z modifies the vertical pressure distribution and thus impact the streamwise momentum balance indirectly. The net effect is a stress force T in the x-direction given by [47, 60]

$$T = -\frac{1}{g}\int_0^h \left(\sigma_x - \sigma_z\right)\mathrm{d}z = -\frac{4}{g}\int_0^h \nu_t\frac{\partial u}{\partial x}\mathrm{d}z \tag{27}$$

It can be simplified for computational purposes as follows

$$T \approx -\frac{4}{g}\nu_t\frac{\partial U}{\partial x}h = \left[\left(\frac{4}{g}\frac{\nu_t}{q}\right)\frac{\partial h}{\partial x}\right]\frac{q^2}{h} = \alpha h_x\frac{q^2}{gh}, \tag{28}$$

where a vertically-averaged eddy viscosity was assumed and $\partial U/\partial x$ was used instead of $\partial u/\partial x$. The streamwise x-momentum balance then reads

$$\frac{\mathrm{d}}{\mathrm{d}x}(S+T) = h\left(S_o - S_f - S_D\right). \tag{29}$$

Now, a suitable approximation to ν_t and hence for α is required. Hosoda and Tada [43] assumed $\alpha=0.05$ by calibrating numerical simulations. However, it is expected that the value of ν_t will depend to some extend on F_1. Thus, a simplified approximation is presented in the ensuing development based on scaling considerations. Using a parabolic depth-distribution of the eddy viscosity [3], its depth averaged value is given by

$$\nu_t = \frac{\kappa}{6}\left(\frac{f}{8}\right)^{1/2} q, \tag{30}$$

where $\kappa=0.41$ is the von Kármán constant. Equation (30) yields reasonable predictions for uniform or gradually-varied open channel flows. However, the flow in undular jumps is rapidly-varied, and Eq. (30) produces small Reynolds stresses. Madsen et al. [63] conducted detailed turbulence measurements in weak hydraulic jumps, and found that the normalized eddy viscosity Λ at the interface of the main stream and the roller

$$\Lambda = \frac{\nu_t}{qR^2}, \tag{31}$$

is of the order of 10^{-3}, albeit with some scatter, with $R=h_2/h_1$ as the sequent depth ratio of the hydraulic jump. Interestingly, the order of this normalized eddy viscosity is similar to that obtained from Eq. (30) for typical values, e.g. $f=0.015$. Note that for $R=1$, either representing subcritical uniform flow or supercritical uniform, R plays no role as scaling in Eq. (31), and one gets simply using Eq. (30)

$$\Lambda = \frac{\kappa}{6}\left(\frac{f}{8}\right)^{1/2}. \tag{32}$$

Thus, one may assume that the basic scaling for the depth-averaged eddy-viscosity within the hydraulic jump is R^2. Therefore, the following approximation is adopted to compute a depth-averaged eddy viscosity in the undular jump ($R>1$) based on the basic values for gradually-varied flows,

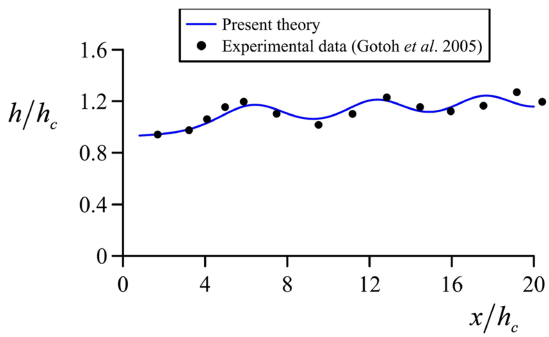

Fig. 6 Free surface profile $h/h_c[x/h_c]$ of an undular hydraulic jump for $\mathrm{F}_1=1.11$ and $S_o=1/282$, with the critical depth $h_c=(q^2/g)^{1/3}$ as scaling

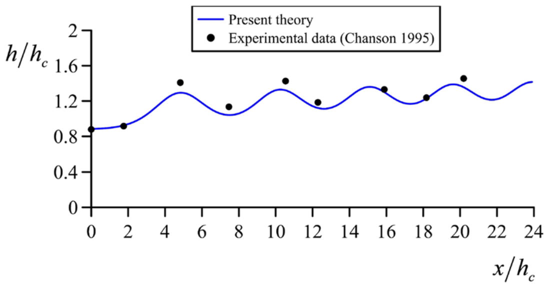

Fig. 7 Free surface profile $h/h_c[x/h_c]$ of an undular hydraulic jump for $F_1=1.21$ and $S_o=0.005672$, with the critical depth $h_c=(q^2/g)^{1/3}$ as scaling

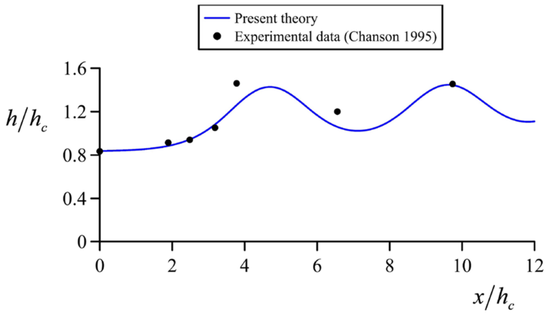

Fig. 8 Free surface profile $h/h_c[x/h_c]$ of an undular hydraulic jump for $F_1=1.31$ and $S_o=0.006667$, with the critical depth $h_c=(q^2/g)^{1/3}$ as scaling

$$\nu_t = \frac{\kappa}{6}\left(\frac{f}{8}\right)^{1/2} q\left\{\frac{1}{4}\left[\left(1+8F_1^2\right)^{1/2}-1\right]^2\right\}, \tag{33}$$

thereby including the effect of F_1 on ν_t. Thus, α is given by

$$\alpha = \frac{\kappa}{6}\left(\frac{f}{8}\right)^{1/2}\left[\left(1+8F_1^2\right)^{1/2}-1\right]^2. \tag{34}$$

This approximation, albeit rude, is however based on scaling reasoning and give estimates of α dependent on F_1, on the order of magnitude of the previously calibrated value by Hosoda and Tada [43]. For example, for $f=0.015$ and $F_1=1.5$ one gets $\alpha \approx 0.033$. Therefore, for depth-averaged modeling purposes it is adopted without any further refinement.

5 Test cases

The measured free surface profile of an undular hydraulic jump for $F_1=q/(gh_1{}^3)^{1/2}=1.11$ in a channel of bottom slope 1/282 is considered in Fig. 6 [35]. This is a type A jump, with a 2D flow structure given the absence of cross-waves. The present depth-averaged Boussinesq model with was numerically solved using the 4$^{\text{th}}$-order Runge Kutta method adopting a power law exponent at the inflow section $N_1=1/7$ as indicated by the experimentally measured inflow velocity profile [35] and $K=2$ based on former curvilinear flow results. It can be observed that the theoretical prediction is in good agreement with experimental results.

Chanson [23] conducted detailed experimental measurement of undular jumps in a tilting rectangular flume of width 0.25 m. The measured free surface profile of an undular

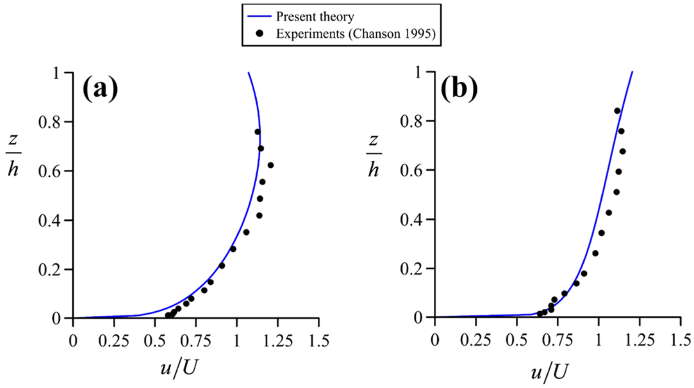

Fig. 9 Velocity profile u/U at first wave **a** crest, **b** trough, for the undular jump with $F_1 = 1.31$ and $S_o = 0.006667$ (Fig. 8)

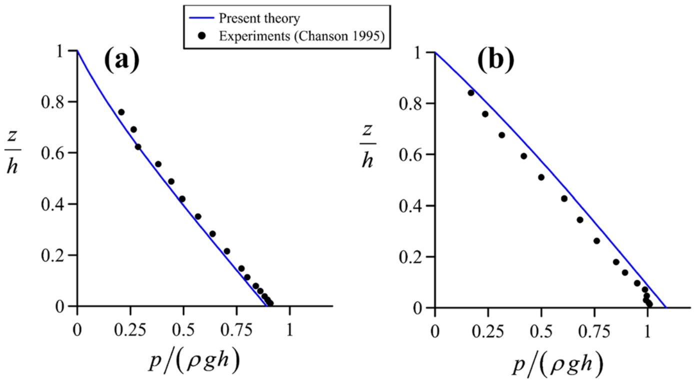

Fig. 10 Pressure distribution $p/(\rho g h)$ at first wave **a** crest, **b** trough, for the undular jump with $F_1 = 1.31$ and $S_o = 0.006667$ (Fig. 8)

Fig. 11 Free surface profile $h/h_c[x/h_c]$ of an undular hydraulic jump for $F_1 = 1.366$ and $S_o = 0.0014$, with the critical depth $h_c = (q^2/g)^{1/3}$ as scaling

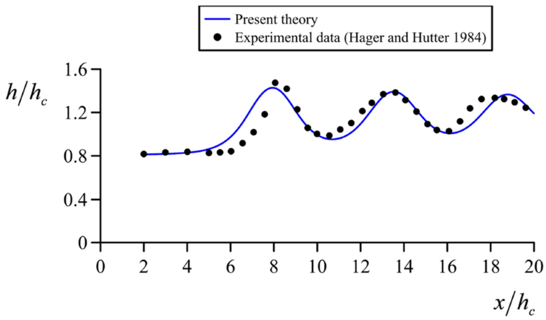

hydraulic jump for $F_1 = 1.21$ ($q = 0.12$ m^2/s) setting the bottom slope to 0.005672 is considered in Fig. 7. The theoretical predictions of the present model using $N_1 = 1/7$ and $K = 2$ are displayed in the same figure, showing fair agreement with observations, albeit with some under- and overpredictions of wave crest and troughs, respectively.

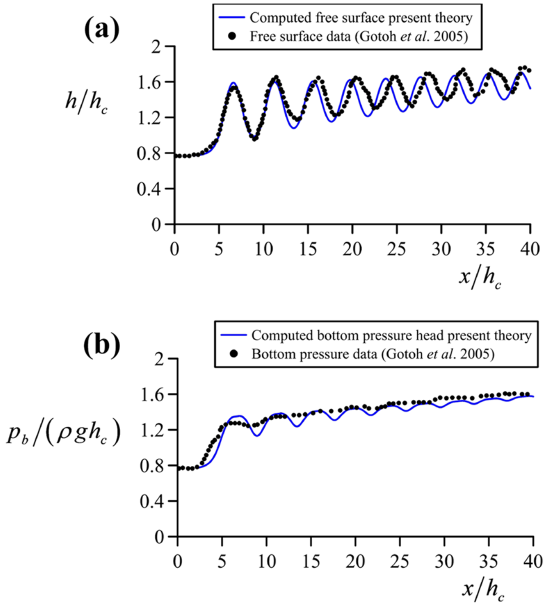

Fig. 12 Free surface profile $h/h_c[x/h_c]$ and bottom pressure head $p_b/(\rho g h_c)[x/h_c]$ of an undular hydraulic jump for $F_1=1.47$ and $S_o=1/163$, with the critical depth $h_c=(q^2/g)^{1/3}$ as scaling

The experimental free surface profile for a test with $F_1=1.31$ ($q=0.1$ m^2/s) and $S_o=0.006667$ [23] is plotted in Fig. 8. The exponent N_1 was settled to 1/9.33 by fitting a power-law profile to the measured velocity profile at the inflow section. This test corresponds to a D type jump given that $y_c/b=0.403$ [23]. Wave breaking and shock waves makes this test, therefore, more challenging for simulation. The theoretical prediction for the free surface profile is compared with the experimental measurements in Fig. 8, showing fair agreement. Note that the ascending branch of the first wave shows a sharp increase in the free surface slope, which is rather smoother in the numerical model.

Predicted and measured velocity profiles at the channel centerline u/U are plotted in Fig. 9 for the first wave crest and trough, whereas the pressure distributions at the same sections are considered in Fig. 10. Overall the predictions of the present theory are in fair agreement with experimental measurements, with better results than those presented with a former model [47].

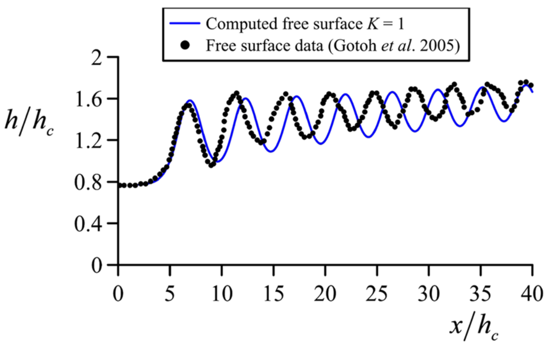

Fig. 13 Free surface profile $h/h_c[x/h_c]$ of an undular hydraulic jump for $F_1=1.366$ and $S_o=0.0014$, using $K=1$

Fig. 14 Free surface profile $h/h_c[x/h_c]$ of an undular hydraulic jump for $F_1 = 1.47$ and $S_o = 1/163$, for **a** Montes and Chanson [30] theory, **b** Serre–Green–Naghdi theory [41]

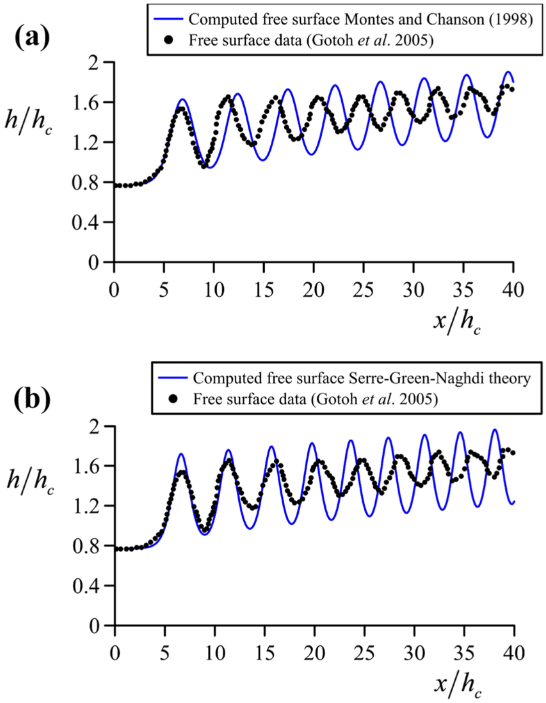

The measured free surface profile of an undular hydraulic jump for $F_1 = 1.366$ ($q = 0.099$ m^2/s) in a channel of bottom slope 0.0014 is considered in Fig. 11 [39]. The theoretical prediction for this experiment was accomplished using $N_1 = 1/10$ and $K = 2$, with the corresponding results presented in Fig. 11. As previously noted in former tests the raise of the first wave is sharper in the experiments than in the numerical simulations. However, the tailwater cnoidal-type waves are excellently predicted by the theoretical model.

The measured free surface profile and bottom pressure head of an undular hydraulic jump for $F_1 = 1.47$ ($q = 0.1$ m^2/s) in a channel of bottom slope 1/163 is considered in Fig. 12 [35]. The theoretical prediction for this experiment was accomplished using $N_1 = 1/7$ and $K = 2$, with the corresponding results presented in Fig. 12. The theoretical prediction for the free surface profile is in good agreement with observations, especially for the two first waves. From the third wave onwards a small phase shift is noted, due to the smaller wave

Fig. 15 Free surface profile $h/h_c[x/h_c]$ of an undular hydraulic jump for $F_1 = 1.366$ and $S_o = 0.0014$, using $K = 2.2$

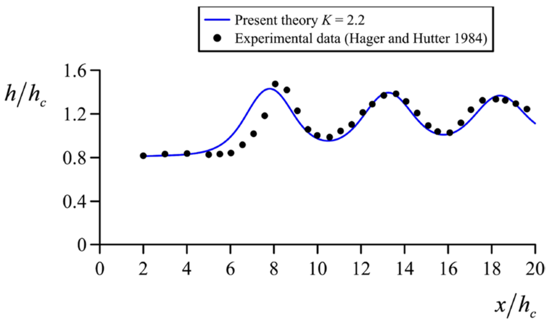

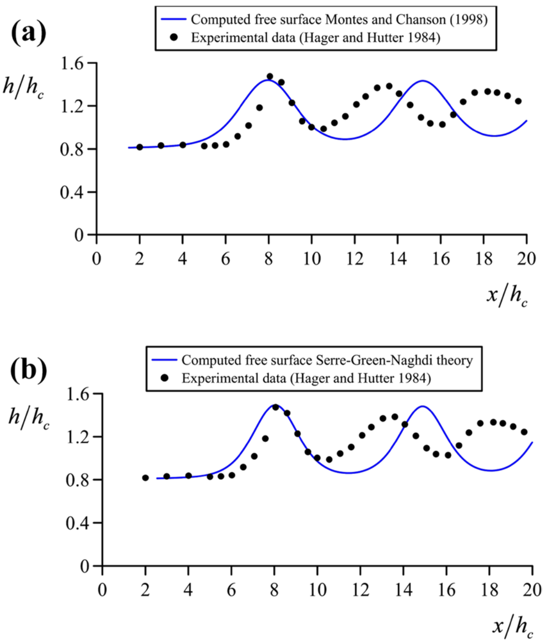

Fig. 16 Free surface profile $h/h_c[x/h_c]$ of an undular hydraulic jump for $F_1 = 1.366$ and $S_o = 0.0014$, for **a** Montes and Chanson [30] theory, **b** Serre–Green–Naghdi theory [41]

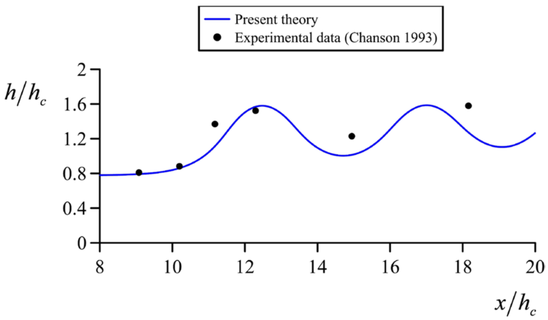

Fig. 17 Free surface profile $h/h_c[x/h_c]$ of an undular hydraulic jump for $F_1 = 1.45$ and $S_o = 0.007599$, with the critical depth $h_c = (q^2/g)^{1/3}$ as scaling

lengths predicted. There are some discrepancies between measured and simulated bottom pressure heads in the ascending branch of the first wave, but the remaining portion of the predicted pressure profile is in reasonable agreement with observations.

The impact of selecting alternative values for K is highlighted in Fig. 13, where the test of Fig. 12 is reconsidered using $K = 1$, as adopted by Montes and Chanson [30]. It can be observed that the effect for the first wave is not significant, but for the third one onwards the phase shift due to an overprediction of wavelengths along the wave train is notable. Thus, the impact of K on the curvilinear flow features is important, with wave lengths significantly affected.

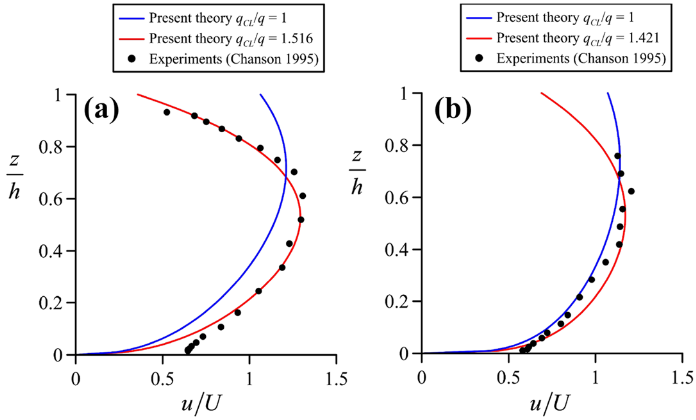

Fig. 18 Velocity profile u/U at first wave of **a** the undular jump with $F_1 = 1.45$ and $S_o = 0.007599$, **b** the undular jump with $F_1 = 1.31$ and $S_o = 0.006667$

6 Discussion: comparison of present theory with other approximations and limitations

In the former section the present theory was compared with detailed experimental measurements from different sources, resulting a fair agreement in all the tests conducted, although it is acknowledged that the comparison was limited to the centerline flow. Now, a comparison with Montes and Chanson [30] and Serre–Green–Naghdi [41] theories is relevant, at the time that some limitations of the new theory are discussed.

The undular jump test of Fig. 12 ($F_1 = 1.47$) is reconsidered in Fig. 14, where both Montes and Chanson (MC) [30] and Serre-Green-Naghdi (SGN) [41] theories were used to produce theoretical solutions. In MC theory $K = 1$ was used, as proposed by them, whereas SGN theory is free from curvilinear flow parameters. Note that both theories produce a first wave crest with some overprediction, whereas over and underpredictions of wave crest and troughs are systematic along the entire wave train. These are more extreme for the SGN theory. However, MC theory produces an overprediction of wave lengths resulting in a notable phase shift for the wave profile. Comparison of the results of the present theory (Fig. 12) with MC and SGN simulations reveals the improved predictions of the former.

Although the benefits of using the new theory are thus evident, its limitations are also to be kept in mind. Besides the inherent limitations of using a depth-averaged model to approximate a complex 3D flow, it was revealed the role of K controlling the wave lengths of the undular jump profile, and the improved selection $K = 2$ as compared to the standard one $K = 1$. Our choice for K was determined rationally based on an approximate analysis of the solitary wave profile. This result shall not be rigidly taken, given that it should be expected to have a variation of K along the wave profile in response to the local flow conditions. So far there is not a general approach to determine this curvature exponent, and former works used either flow net analyses [64] or auxiliary equations as the moment of momentum [65] under ideal fluid flow conditions. However, a corresponding approach for the complex turbulent flow in undular jumps is not available.

Some calibration of results is another option. The undular jump profile presented in Fig. 11 ($F_1 = 1.366$) is reconsidered in Fig. 15 using $K = 2.2$ in the sense of calibration parameter, resulting an improved prediction of the tailwater cnoidal waves, noted in the third wave. However, this practice is not general, such that the particular value of K is unknown in advance. In the lack of theoretical tools to predict K, the approximate value $K=2$ obtained herein by our simplified ideal fluid flow analysis is suggested.

The undular jump test of Fig. 11 is presented again in Fig. 16 for comparison purposes with MC and SGN theories. Note that both MC and SGN models predict a first wave profile very similar to the one obtained using the present theory (see Fig. 11). However, from the first wave onwards the tailwater cnoidal waves are not reproduced with much accuracy neither by MC nor by SGN theories, whereas the new approach produces a good solution.

The experimental free surface profile for a test with $F_1=1.45$ ($q=0.06$ m^2/s) and $S_o=0.007599$ [23] is plotted in Fig. 17. The numerical simulation obtained with the present theory using $N_1=1/8$ and $K=2$ is plotted in the same figure, showing fair agreement with observations.

This test will be used to depict one of the limitations of the present theory, namely the lack of consideration of flow concentration on the centerline. The unit discharge at the centerline q_{CL} showed experimentally a marked undulating pattern in the streamwise direction, mimicking the wave crests and troughs of the jump profile [23]. Predicted and measured velocity profiles below the first wave crest at the channel centerline for this test u/U are plotted in Fig. 18a, revealing a marked divergence. The same computation was conducted for the undular jump of Fig. 8, although in this case the divergence is less evident. Note that the present theory is based upon $q_{CL}/q=1$, whereas this ratio is 1.516 and 1.421 experimentally for the two wave crests considered!. Therefore, although the predicted centerline free surface profile is not largely affected by this effect, the velocity profile showed a marked redistribution. Part of this redistribution at and just below the free surface may be produced by the wave breaking, but comparison of measurements and predictions also indicates a significant redistribution at the lower portion of the velocity profile, near the channel bottom. Basically, it seeds the idea that streamline curvature effects are larger in the measured velocity profile than in the theoretically predicted. This reasoning agrees with having $q_{CL}/q>1$: if the unit discharge is larger, streamline curvature effects are larger too. Therefore, a main conclusion from this critical comparison is that the flow concentration at the centerline produces an increased streamline curvature effect above that expected based on q.

To test this finding, an approximate theoretical approach to account for the increased streamline curvature at the first wave crest is developed as follows. If the first wave is approximated by a solitary wave, elementary manipulation of the extended Bernoulli equation (Eq. 7) for potential flow ($N=0$) permits to write

$$\frac{2\varepsilon_0}{K+2} = 2F_1^2 - F_1^4 - 1, \tag{35}$$

where the first wave crest flow depth was approximated as $h_M=h_1{F_1}^2$. This relation permits to express the flow curvature effects at the first wave crest as function of approach flow conditions F_1 (or q, given h_1). Therefore, the increase of flow curvature for an increase in q can be approximately estimated. Thus, the following expression was used to obtain the curvature term at the centerline CL

$$\frac{\left(\varepsilon_0\right)_{CL}}{\varepsilon_0} = \frac{1}{4}\left[\frac{2F_{CL}^2 - F_{CL}^4 - 1}{2F_1^2 - F_1^4 - 1}\right], \tag{36}$$

where the factor ¼ is empirical, $F_1 = q/(gh_1^3)^{1/2}$ and $F_{CL} = q_{CL}/(gh_1^3)^{1/2}$. This ratio was used to recompute the velocity profiles, and the results are presented in Fig. 18, showing fair agreement with experiments. Therefore, although the computation is rough and only approximate, with its validity limited to the first wave crest, it does a good service depicting how streamline curvature effects are amplified below the first wave crest by flow concentration.

Shock waves contributes to some flow concentration along the channel centerline, as shown experimentally with flow visualizations [31, 66, 67]. Experimental data showed that the angle to the shock waves with the sidewalls increased with increasing Froude number F_1 [52]. Thus, flow concentration is expected to be stronger with increasing F_1. The lateral velocity component normal to the channel walls is therefore contributing to the increase in unit discharge q along the centerline. However, the basic characteristics of these cross waves are not in strong agreement with the Ippen-Harleman theory [11], such that a simple model for the 2D wave structure is not presently available.

Another types of significant 3D features linked to the velocity profile redistribution are the recirculation flow zones. There are two main different types of recirculation observed in laboratory conditions, besides the surface rollers due to wave breaking: (i) surface recirculation cells immediately behind the shock wave inception, typically with a vertical axis [11, 59, 66] (see Fig. 2), and (ii) bottom recirculation beneath the 1st wave crest, and sometimes beneath 2nd and 3rd wave crests with smaller dimensions, typically with a horizontal axis perpendicular to the main flow direction. The latter recirculation bubble may be observed without any surface roller, but only when the inflow is partially developed as in [24, 31, 68]. Basically, the decelerating flow cause recirculation bubbles beneath the 1st wave crest, with the recirculation effect diminishing towards the sidewalls. A 3rd kind of recirculation in undular jumps are the bottom corner eddies, with longitudinal axis, at the wave crests. These are much smaller and have lesser influence in the flow overall [11, 59]. The recirculation flow zones may be considered as dead-zones (or dead-water volumes) with static pressure and zero mass flux. Thus, the inclusion in depth-averaged flow models may be accomplished considering them as virtual channel boundaries [64]. The spatial dimensions of these flow geometry elements were rarely documented such that their lack of consideration constitute another source of inaccuracy of the current depth-averaged modeling approaches.

7 Conclusions

The existing Boussinesq models to simulate undular hydraulic jumps are limited to $F_1 < 1.2$, or, equivalently, to 2D wavy free surface flow, given that some relevant 3D flow effects, namely the shock-wave drag, turbulent breaking and turbulent stresses, are not accounted for. In this work, a depth-averaged Boussinesq model which approximately accounted for 3D flow effects was presented. The model is based on a former 2D Boussinesq-type approach with boundary shear effects by MC [30]; additions consist in a drag slope due to shock waves, turbulent breaking for attenuation of non-hydrostaticity and a eddy viscosity approach for the turbulent stresses. To the Authors' knowledge, this model is the first attempt in the literature to include all these effects in the Boussinesq-type framework for modeling stationary undular hydraulic jumps.

The model predictions were compared with experimental results from different sources for $F_1 < 1.5$ resulting a reasonable agreement, thereby indicating its utility to predict jump types A, B, C and D. It cannot be applied to type E jumps, given that turbulent breaking is only approximately accounted for, and surface rollers are not mathematically modeled.

It was found that the curvature distribution parameter has a significant effect controlling the wave length, and an approximate value was obtained based on ideal fluid flow computations of solitary waves. A general method, however, is still missing and the proposed $K=2$ shall be therefore considered in the lack of a more refined approach. The new depth-averaged model equations does not include the effect of flow concentration in the centerline. This 3D feature produces an increased curvature effect on the velocity profiles. It was analysed at the first wave crest based on an improved (simplified) treatment of flow curvature accounting for the centerline discharge q_{CL}, resulting in better velocity profile predictions. Simply, the flow concentration observed experimentally on the channel centerline is a major physical feature in stationary undular hydraulic jumps. Although the development is not general and cannot be included in the general depth-averaged computations, it highlights the impact of the ratio q_{CL}/q on the velocity profile features.

The main limitation of the new model presented in this critical review relies on approximating a complex 3D flow by an approximate depth-averaged model. However, even with this limitation in mind, the new predictions obtained with our approximate treatment of 3D effects are significantly better than those obtainable with previous formulations.

Appendix: Development of 2D Boussinesq equations with boundary shear

The viscous velocity distribution for two-dimensional wavy free surface flow is [30]

$$V = V_s \mu^N \exp\left(-\varepsilon_0 \frac{1-\mu^{K+1}}{K+1}\right), \tag{37}$$

where V_s is the velocity at the free surface, $\mu = z/h$, z the elevation, h the flow depth, K the curvature parameter, N the power-law exponent, $h_x = \mathrm{d}h/\mathrm{d}x$ and $h_{xx} = \mathrm{d}^2h/\mathrm{d}x^2$ and $\varepsilon_0 = hh_{xx}/(1+h_x{}^2)$. For small arguments of the exponential function, Eq. (37) is approximated by

$$V = V_s \mu^N \exp\left(-\varepsilon_0 \frac{1-\mu^{K+1}}{K+1}\right) \approx V_s \mu^N \left(1 - \varepsilon_0 \frac{1-\mu^{K+1}}{K+1}\right). \tag{38}$$

Projection of this result into the (x, z) directions yields the velocity components (u, v) [30]

$$u \approx (1+N)\frac{q}{h}\mu^N \left[1 - \frac{\varepsilon_0}{K+1}\left(\frac{1+N}{K+2+N} - \mu^{K+1}\right) - \frac{\varepsilon_1}{2}\left(\frac{N+1}{N+3} + \mu^2\right)\right], \tag{39}$$

$$v \approx (1+N)\frac{q}{h}\mu^{N+1}\varepsilon_1^{1/2}\left[1 - \frac{\varepsilon_0}{K+1}\left(\frac{1+N}{K+2+N} - \mu^{K+1}\right) - \frac{\varepsilon_1}{2}\frac{N+1}{N+3}\right], \tag{40}$$

and the pressure distribution

$$\frac{p}{\rho gh}=1-\mu+\frac{\varepsilon_0(1+N)^2}{K+2N+1}\frac{q^2}{gh^3}\left(1-\mu^{1+2N+K}\right), \tag{41}$$

where $\varepsilon_1 = {h_x}^2/(1+{h_x}^2)$. Now, the specific momentum S is given by

$$S=\int_0^h\left(\frac{V^2}{g}+\frac{p}{\rho g}\right)\mathrm{d}z. \tag{42}$$

From Eq. (38)

$$V^2\approx(1+N)^2\frac{q^2}{h^2}\mu^{2N}\left[1-\frac{2\varepsilon_0}{K+1}\left(\frac{1+N}{K+2+N}-\mu^{K+1}\right)-\varepsilon_1\frac{N+1}{N+3}\right]. \tag{43}$$

Integration of Eq. (43) yields

$$\int_0^h\frac{V^2}{g}\mathrm{d}z=(1+N)^2\frac{q^2}{gh}\left(\frac{1}{2N+1}-\frac{2\varepsilon_0}{K+1}\left(\frac{1+N}{K+2+N}\frac{1}{2N+1}-\frac{1}{K+2N+2}\right)-\varepsilon_1\frac{N+1}{N+3}\frac{1}{2N+1}\right) \tag{44}$$

After manipulation, Eq. (44) is rewritten as

$$\int_0^h\frac{V^2}{g}\mathrm{d}z=\beta\frac{q^2}{gh}\left(1-\frac{2\varepsilon_0}{K+1}\left(\frac{1+N}{K+2+N}-\frac{2N+1}{K+2N+2}\right)-\varepsilon_1\frac{N+1}{N+3}\right), \tag{45}$$

where β is the Boussinesq momentum velocity correction coefficient for the power-law velocity profile,

$$\beta=\frac{(1+N)^2}{2N+1}. \tag{46}$$

Using Eq. (41) one obtains

$$\int_0^h\frac{p}{\rho g}\mathrm{d}z=\frac{h^2}{2}+\frac{\varepsilon_0(1+N)^2}{K+2N+1}\frac{q^2}{gh}\left(1-\frac{1}{2+2N+K}\right)=\frac{h^2}{2}+\beta\varepsilon_0\frac{2N+1}{K+2N+2}\frac{q^2}{gh}. \tag{47}$$

Inserting Eqs. (45) and (47) in Eq. (42) yields for the specific momentum S

$$\begin{aligned}
S&=\beta\frac{q^2}{gh}\left(1-\frac{2\varepsilon_0}{K+1}\left(\frac{1+N}{K+2+N}-\frac{2N+1}{K+2+2N}\right)-\varepsilon_1\frac{N+1}{N+3}\right)+\frac{h^2}{2}+\beta\varepsilon_0\frac{2N+1}{K+2N+2}\frac{q^2}{gh}\\
&=\frac{h^2}{2}+\beta\frac{q^2}{gh}\left(1+\varepsilon_0\left(\frac{2N+1}{K+2+2N}-\frac{2(N+1)}{(K+1)(K+2+N)}+\frac{2(1+2N)}{(K+1)(K+2+2N)}\right)-\varepsilon_1\frac{N+1}{N+3}\right)\\
&=\frac{h^2}{2}+\beta\frac{q^2}{gh}\left(1+\varepsilon_0\left(\frac{2}{K+2+N}+\frac{2NK^2-K^2+2N^2K+5NK-3K+2N^2+3N-2}{(K+1)(K+N+2)(K+2+2N)}\right)-\varepsilon_1\frac{N+1}{N+3}\right)\\
&=\frac{h^2}{2}+\beta\frac{q^2}{gh}\left(1+\varepsilon_0\left(\frac{2}{K+2+N}-\frac{1-2N}{K+2+2N}\right)-\varepsilon_1\frac{N+1}{N+3}\right).
\end{aligned} \tag{48}$$

The depth-averaged specific energy head E is

$$E=\frac{1}{h}\int_{0}^{h}\left(\frac{V^2}{2g}+\frac{p}{\rho g}+z\right)\mathrm{d}z. \tag{49}$$

Using Eqs. (45) and (47), Eq. (49) yields

$$\begin{aligned}
E&=h+\beta\frac{q^2}{2gh^2}\left(1-\frac{2\varepsilon_0}{K+1}\left(\frac{1+N}{K+2+N}-\frac{2N+1}{K+2N+2}\right)+2\varepsilon_0\frac{2N+1}{K+2N+2}-\varepsilon_1\frac{N+1}{N+3}\right)\\
&=h+\beta\frac{q^2}{2gh^2}\left(1+\frac{2\varepsilon_0}{K+2N+2}\left(\frac{2N+1}{K+1}-\frac{(N+1)(K+2N+2)}{(K+N+2)(K+1)}+2N+1\right)-\varepsilon_1\frac{N+1}{N+3}\right)\\
&=h+\beta\frac{q^2}{2gh^2}\left(1+\frac{2\varepsilon_0}{K+2N+2}\left(\frac{N}{K+N+2}+2N+1\right)-\varepsilon_1\frac{N+1}{N+3}\right)\\
&=h+\beta\frac{q^2}{2gh^2}\left(1+\frac{2\varepsilon_0}{K+2N+2}\left(1+N\left(2+\frac{1}{K+N+2}\right)\right)-\varepsilon_1\frac{N+1}{N+3}\right).
\end{aligned} \tag{50}$$

Equations (48) and (50) are the extended momentum and energy equations for viscous wavy free surface flow. Some typos in the original paper by Montes and Chanson [30] makes the detailed derivation presented here useful.

Acknowledgements The Authors would like to dedicate this article to Prof. J. Sergio Montes, University of Hobart, Tasmania. His work had a deep impact on the Authors' own work, and the results presented in this research were possible thanks to his pioneering contributions. The Authors would like to express their gratitude to the SI Editor, Prof. Subhasish Dey, for his invitation to prepare this review article. The work of the first Author was supported by the Spanish project VAMONOS (CTM2017-85171- C2-1-R) and grant María de Maeztu for Centers and Units of Excellence in R&D (Ref. CEX2019-000968-M).

References

1. Montes JS (1986) A study of the undular jump profile. In: 9th Australasian Fluid Mechanic Conference Auckland, 148–151.
2. Montes JS (1998) Hydraulics of open channel flow. ASCE Press, Reston
3. Chanson H (2004) The hydraulics of open channel flows: an introduction. Butterworth-Heinemann, Oxford
4. Chanson H (2010) Undular tidal bores: basic theory and free-surface characteristics. J Hydraul Eng ASCE 136(11):940–944. https://doi.org/10.1061/(ASCE)HY.1943-7900.0000264
5. Castro-Orgaz O, Hager WH (2019) Shallow water hydraulics. Doi: https://doi.org/10.1007/978-3-030-13073-2, 563 pages, Springer, Berlin
6. Chanson H (1996) Free-surface flows with near-critical flow conditions. Can J Civ Eng 23(6):1272–1284. https://doi.org/10.1139/l96-936
7. Lemoine R (1948) Sur les Ondes Positives de Translation dans les Canaux et sur le Ressaut Ondulé de Faible Amplitude. (On the Positive Surges in Channels and on the Undular Jumps of Low Wave Height.) Jl La Houille Blanche, 183–185 (in French)
8. Riquois R, Ract-Madoux X (1965) Intumescences Observées sur le Canal d'Amenée de la Chute d'Oraison lors des Variations Rapides de Charge. (Surges observed in the Oraison Hydropower Canal during Rapid Discharge Variations.). In: Proceedings of 11th IAHR Biennial Congress, Leningrad, Russia, paper 3.53, 15 pages (in French)
9. Cunge JA (1966) Comparaison des Résultats des Essais d'Intumescences Effectués sur le Modèle Réduit et sur le Modèle Mathématique du Canal Oraison-Manosque. (Comparison of Positive Surge Results between Physical Modelling and Numerical Modelling of the Oraison-Manosque Canal.) Journal La Houille Blanche, No. 1, 55–69 & 79 (In French)
10. Treske A (1994) Undular Bores (Favre-Waves) in open channels - experimental studies. J Hydraul Res IAHR, 32(3): 355–370. Discussion: 33(3), 274–278, 1995

11. Chanson H, Montes JS (1995) Characteristics of undular hydraulic jumps: experimental apparatus and flow patterns. J Hydraulic Eng 121(2): 129–144; 123(2), 161–164
12. Koch C, Chanson H (2008) Turbulent mixing beneath an undular bore front. J Coastal Res 24(4):999–1007. https://doi.org/10.2112/06-0688.1
13. Serre F (1953) Contribution à l'étude des écoulements permanents et variables dans les canaux (Contribution to the study of steady and unsteady channel flows). La Houille Blanche 8(6–7), 374–388; 8(12), 830–887 (in French)
14. Green AE, Naghdi PM (1976) Directed fluid sheets. Proc R Soc Lond A 347:447–473
15. Green AE, Naghdi PM (1976) A derivation of equations for wave propagation in water of variable depth. J Fluid Mech 78:237–246
16. Su CH, Gardner CS (1969) KDV equation and generalizations. Part III. Derivation of Korteweg-de Vries equation and Burgers equation. J Math Phys 10(3): 536–539
17. Wei G, Kirby JT, Grilli ST, Subramanya R (1995) A fully nonlinear Boussinesq model for surface waves 1: highly nonlinear unsteady waves. J Fluid Mech 294:71–92
18. Marchi E (1963) Contributo allo studio del risalto ondulato (Contribution to the study of undular jumps). Giornale del Genio Civile 101(9):466–476 (in Italian)
19. Keulegan GH, Patterson GW (1940) Mathematical theory of irrotational translation waves. J Res Nat Bur Stand 24(1):47–101
20. Peregrine DH (1966) Calculations of the development of an undular bore. J Fluid Mech 25(2):321–330
21. Peregrine DH (1967) Long waves on a beach. J Fluid Mech 27(5):815–827
22. Castro-Orgaz O, Chanson H (2020) Undular and broken surges in dam-break flows: a review of wave breaking strategies in a Boussinesq-type framework. Environ Fluid Mech 20(6):1383–1416
23. Chanson, H. (1995). Flow characteristics of undular hydraulic jumps: Comparison with near-critical flows. Res. Rep. CH45/95. Dept. Civ. Engng., The University of Queensland, Brisbane, Australia
24. Donnelly C, Chanson H (2005) Environmental Impact of Undular Tidal Bores in Tropical Rivers. Environ Fluid Mech 5(5):481–494. https://doi.org/10.1007/s10652-005-0711-0
25. Rouse H (1938) Fluid mechanics for hydraulic engineers. McGraw-Hill, New York
26. Liggett JA (1994) Fluid mechanics. McGraw-Hill, New York
27. Chanson H (2011) Tidal Bores, Aegir, Eagre, Mascaret, Pororoca: Theory and Observations. World Scientific, Singapore, 220 pages. ISBN: 978-981-4335-41-6/981-4335-41-X
28. Chanson H (2000) Boundary shear stress measurements in undular flows: application to standing wave bed forms. Water Resour Res 36(10):3063–3076. https://doi.org/10.1029/2000WR900154
29. Fawer C (1937) Étude de quelques écoulements permanents à filets courbes (Study of some steady flows with curved streamlines). *Thesis*, Université de Lausanne. La Concorde, Lausanne (in French)
30. Montes JS, Chanson H (1998) Characteristics of undular hydraulic jumps: results and calculations. J Hydraul Eng 124(2):192–205
31. Ohtsu I, Yasuda Y, Gotoh H (2001) Hydraulic condition for undular jump formations. J Hydraul Res 39(2): 203–209; 40(3), 379–384
32. Ben Meftah M, De Serio F, Mossa M, Pollio A (2007) Analysis of the velocity field in a large rectangular channel with lateral shockwave. Environ Fluid Mech 7(6):519–536. https://doi.org/10.1007/s10652-007-9034-7
33. Reinauer R, Hager WH (1995) Non-breaking undular hydraulic jump. J Hydraul Res 33(5): 1–16; 34(2): 279–287; 34(4): 567–573
34. Ohtsu I, Yasuda Y, Gotoh H (2003) Flow conditions of undular hydraulic jumps in horizontal rectangular channels. J Hydraul Eng 129(12):948–955
35. Gotoh H, Yasuda Y, Ohtsu I (2005) Effect of channel slope on flow characteristics of undular hydraulic jumps. Trans Ecol Environ 83(1):33–42
36. Boussinesq J (1877) Essai sur la théorie des eaux courantes (Essay on the theory of flowing water). Mémoires présentés par Divers Savants á l'Académie des Sciences Paris 23(1):1–608 (in French)
37. Iwasa Y (1955) Undular jump and its limiting conditions for existence. In: Proceedings of 5th Japan National Congress Applied Mechanic II(14), 315–319
38. Mandrup-Andersen, V. (1978). Undular hydraulic jump. J. Hydrau Div ASCE 104(HY8), 1185–1188; 105(HY9), 1208–1211
39. Hager WH, Hutter K (1984) On pseudo-uniform flow in open channel hydraulics. Acta Mech 53(3–4):183–200
40. Benjamin TB, Lighthill MJ (1954) On cnoidal waves and bores. Proc Roy Soc Lond A 224:448–460
41. Castro-Orgaz O, Chanson H (2011) Near-critical free-surface flows: Real fluid flow analysis. Environ Fluid Mech 11(5):499–516
42. Bose S, Castro-Orgaz O, Dey S (2012) Free surface profiles of undular hydraulic jumps. J Hydr Eng 138(4):362–366

43. Hosoda T, Tada A (1994) Free surface profile analysis on open channel flow by means of 1-D basic equations with effect of vertical acceleration. Annu J Hydraul Eng JSCE 38:457–462 (in Japanese)
44. Hosoda, T., Muramoto, Y., Miyamoto, M. (1997). Bottom shear stress of flows over a wavy bed by using depth averaged flow equations. J Hydraul Environ Eng JSCE, 558/II-38, 81–89 (in Japanese)
45. Grillhofer W, Schneider W (2003) The undular hydraulic jump in turbulent open channel flow at large Reynolds numbers. Phys Fluids 15(3):730–735
46. Castro-Orgaz O (2010) Weakly undular hydraulic jump: effects of friction. J Hydraul Res 48(4):453–465
47. Castro-Orgaz O, Hager WH, Dey S (2015) Depth-averaged model for the undular hydraulic jump. J Hydraul Res 53(3):351–363
48. Castro-Orgaz O, Hager WH (2011) Vorticity equation for the streamline and the velocity profile. J Hydraul Res 49(6):775–783
49. Furuya Y, Nakamura L (1968) A semi-integrated momentum method for the auxiliary equation. In: Proceedings of Stanford conference AFOSR-IFP computation of boundary layers 1, 235–246
50. White FM (1991) Viscous fluid flow. McGraw-Hill, New York
51. Chaudhry MH (2008) Open-channel flow, 2nd edn. Springer, New York
52. Chanson, H. (2009). Current knowledge. In: Hydraulic jumps and related phenomena. a survey of experimental results. Eur J Mech B/Fluids, 28(2), 191–210. doi: https://doi.org/10.1016/j.euromechflu.2008.06.004
53. Iwasa Y (1956) Analytical considerations on cnoidal and solitary waves. *Memoires* Faculty of Engineering, Kyoto University 17(4): 264–276
54. Carter JD, Cienfuegos R (2011) The kinematics and stability of solitary and cnoidal wave solutions of the Serre equations. Eur J Mech B/Fluids 30(3):259–268
55. Tanaka M (1986) The stability of solitary waves. Phys Fluids 29:650–655
56. Boadway JD (1976) Transformation of elliptic partial differential equations for solving two dimensional boundary value problems in fluid flow. Int J Num Meth Engng 10(3):527–533
57. Montes JS (1992) A potential flow solution for the free overfall. Proc ICE 96(6): 259–266; 112(1): 85–87
58. Montes JS (1994) Potential flow solution to the 2D transition form mild to steep slope. J Hydraul Eng 120(5): 601–621, 121(9): 681–682
59. Chanson, H. (1993). Characteristics of Undular Hydraulic Jumps. *Research Report No. CE146*, Dept. of Civil Engineering, The University of Queensland, Brisbane, Australia, 109 pages.
60. Khan AA, Steffler P (1996) Physically-based hydraulic jump model for depth-averaged computations. J Hydraul Eng 122(10):540–548
61. Cantero-Chinchilla FN, Bergillos RJ, Gamero P, Castro-Orgaz O, Cea L, Hager WH (2020) Vertically-averaged and moment equations for dam-break wave modeling: shallow water hypotheses. Water 12(11):3232. https://doi.org/10.3390/w12113232
62. Rodi W (1993) Turbulence models and their application in hydraulics, 3rd edn. IAHR Monograph, Balkema
63. Svedsen IA, Veeramony J, Bakunin J, Kirby JT (2000) The flow in weak turbulent hydraulic jumps. J Fluid Mech 418:25–57
64. Castro-Orgaz O (2010) Approximate modeling of 2D curvilinear open channel flows. J Hydraulic Res 48(2):213–224
65. Castro-Orgaz O, Hager WH (2010) Moment of momentum equation for curvilinear free-surface flow. J Hydraul Res 48(5):620–631
66. Imai S, Nakagawa T (1992) On transverse variation of velocity and bed shear stress in hydraulic jumps in a rectangular open channel. Acta Mech 93:191–203
67. Chanson H (1995) Ressaut Hydraulique Ondulé: Mythes et Réalités. (Undular Hydraulic Jump: Myths and Realities). J La Houille Blanche (7), 4–65. doi:https://doi.org/10.1051/lhb/1995068
68. Chanson H (2005) Physical modelling of the flow field in an undular tidal bore. J Hydraul Res 43(3):234–244